Footprints of mesoscale eddy passages in the Strait of Otranto (Adriatic Sea)

Laura Ursella,[1] Vedrana Kovačević,[1] and Miroslav Gačić[1]

Received 8 September 2010; revised 7 December 2010; accepted 29 December 2010; published 8 April 2011.

[1] The footprints of mesoscale eddies propagating through the Strait of Otranto are documented from current meter records, and their formation mechanism is hypothesized. Bottom-mounted Acoustic Doppler Current Profilers data, collected during 5 months (November 2006 through April 2007) at a transect in the core of the outflowing Adriatic Dense Water, reveal energetic events that manifest as vertically uniform current vector rotations on a time scale of about 10 days. At the two moorings close to the center of the strait, coherent current vector rotations were in opposite senses. Simulation of the passage of an idealized cyclonic or anticyclonic rigid circular eddy confirms that these opposed rotations could be associated with passages of eddies in the southward direction. Characteristic parameters of the eddies were estimated: the duration was several days, the peak azimuthal velocity was around 10–20 cm/s, and advection velocity below 15 cm/s was predominantly in the southwestward direction. Cyclones were bigger (diameter 30–36 km) than anticyclones (14–24 km), and they traveled at greater depths. The eddy passage left a prominent signal in the thermohaline and turbidity properties. This latter is probably due to sediment resuspension by strong currents and to the advection of the suspended particles through an upstream located canyon. The eddy formation is explained in terms of stretching of the high potential vorticity water column outflowing the Strait of Otranto, a mechanism similar to that observed in the Denmark Strait overflow. Another possible explanation is the baroclinic instability of the overflow layer which results in the eddy formation.

Citation: Ursella, L., V. Kovačević, and M. Gačić (2011), Footprints of mesoscale eddy passages in the Strait of Otranto (Adriatic Sea), *J. Geophys. Res.*, *116*, C04005, doi:10.1029/2010JC006633.

1. Introduction

[2] The Strait of Otranto is a channel about 70 km wide and 800 m deep connecting the Adriatic and the Ionian Seas (Mediterranean). On average, inflow takes place along the eastern coast while the outflowing current occurs along the western flank of the channel. The surface separating the outflow from the inflow is sloped and intersects the sea surface closer to the western coast; therefore both vertical shear and cyclonic curl are present in the flow field [*Kovačević et al.*, 1999]. The vertical current pattern varies on a variety of timescales from interannual to tidal ones. Previous observational studies in the Strait of Otranto [*Ferentinos and Kastanos*, 1988; *Kastanos and Ferentinos*, 1991] have presented evidence of unstable flow in the shear zone between the northward and southward currents. This variability has been explained in terms of the near-inertial waves and mesoscale eddies. According to the authors, eddies rotate counterclockwise, propagate northward and pass over the measurement area, appearing as a 10 day variability in the Eulerian current record. The typical dimensions of mesoscale eddies are several internal radii of deformation. In the Adriatic Sea the baroclinic radius of deformation is ~5 km.

[3] Mesoscale eddies in general play an important role in transferring particles, nutrients and other passive material vertically or horizontally [*Williams and Follows*, 1998]. There is an ample experimental evidence of mesoscale eddies from the Labrador Sea [*Lilly and Rhines*, 2002, and references therein]. Large mesoscale variability and eddy formation associated with the overflow currents in the Denmark Strait [*Bruce*, 1995] have been observed, and they have also been produced in laboratory experiments [*Whitehead et al.*, 1990]. The eddy formation in the strait overflow has been explained in terms of the stretching of the high potential vorticity water column due to the dense overflow water descending the continental slope [*Spall and Price*, 1998]. *Kida et al.* [2009, and references therein] used a two-layer isopycnal model to simulate the eddy variability observed when marginal seas overflows enter the open ocean. The model shows that the baroclinic instability of the overflow manifests as eddy variability along the whole water column. Mesoscale eddies are responsible for the entrainment in the dense water overflow plume [*Voet and Quadfasel*, 2010]. Within the western

[1]Istituto Nazionale di Oceanografia e di Geofisica Sperimentale, Sgonico, Italy.

0148-0227/11/2010JC006633

portion of the Strait of Otranto, outflow of the Adriatic Dense Water (AdDW) occurs as a density-driven current in the bottom layer pressed against the continental margin [*Gačić et al.*, 1996; *Manca et al.*, 2002]. The Strait of Otranto is thus an area where the eddy formation can take place. These eddies can then be responsible for the exchange between the shelf and open sea area and should contribute to the AdDW outflow by entrainment processes.

[4] Here we present a detailed analysis in the time and frequency domain of the long-term current records in the outflowing vein of the AdDW in the Strait of Otranto. We attempt to explain current vectors' rotational events of the synoptic timescale band (10 days) hypothesizing the mesoscale eddy passages over the mooring array. We assume that the eddy formation mechanism can be either stretching of the high potential vorticity water column or baroclinic instability. The eddy parameters (such as peak azimuthal velocity, diameter, advection speed and direction) are estimated according to *Lilly and Rhines* [2002], and compared with the simulated theoretical results.

[5] The manuscript is organized as follows: in section 2 we briefly report the mooring configuration, data treatment and time series analysis carried out on the available data sets. In section 3 results regarding the rotational events observed in the current meter data, and associated with the variability in temperature, salinity and turbidity records, are discussed. The observed current variations are compared to the effects provoked by the passage of the idealized eddies in section 4. Calculation of eddy parameters is given in section 5. Thermohaline properties are presented in section 6. Finally, section 7 summarizes the observational evidence and discusses a hypothetical mechanism for the eddy formation.

2. Data and Methods

[6] The deep-current data set we explore consists of a total of three moorings that were deployed in the Strait of Otranto (Figure 1), in the bottom layer of the westernmost portion of the cross section and inside the core of the AdDW, the outflowing density-driven current. The data used in this paper are from the vulnerabilità delle coste e degli ecosistemi marini italiani ai cambiamenti climatici e loro ruolo nei cicli del carbonio mediterraneo (VECTOR) project and are fully described in the paper of *Ursella et al.* [2011].

[7] The moorings were equipped with an Aanderaa current meter 17 m above the seabed, CT (Conductivity-Temperature) SBE37 probes 2 m above the current meter and an upward looking RDI ADCP (Acoustic Doppler Current Profiler) 10 m above the CT. The Aanderaa current meter at station V4 was also equipped with a turbidity sensor. The sampling interval was set to 30 min for the current meters and the turbidity sensor and to 15 min for the ADCPs and the CTs. The ADCP measurements covered layers about 100 m thick at station V3 (22 cells of 5 m each), about 80 m thick at V2 (16 cells of 5 m) and 60 m at V4 (12 cells of 5 m). The moorings were deployed in mid-November 2006 and were recovered in mid-April 2007. All data, except the currents from the Aanderaa current meter at station V3, were successfully retrieved.

[8] For all the analysis considered herein, each cell of the ADCP was treated as an individual time series. Current vectors were decomposed into u (eastward, zonal) and v (northward, meridional) components. Tidal constituents, obtained from harmonic analysis, with signal-to-noise ratio > 1, were subtracted to detide the time series. Finally, a low-pass filter with cut-off period at 33 h [*Flagg et al.*, 1976] was applied in order to remove inertial oscillations, thus obtaining subinertial nontidal flow, from now on referred to as subtidal flow. The time series of potential temperature (θ) and salinity (S), as well as the potential density anomaly ($\sigma_0 = \rho_\theta - 1000$ kg/m^3, where ρ_θ is the potential density of the seawater) termed 'density' from now on, all derived from the CT sensors, were treated in the same way to obtain low-frequency records. The CTD (Conductivity-Temperature-Depth) casts conducted during the mooring deployment (November 2006) and recovery operations (April 2007), as well as those at the representative station from the Southern Adriatic Pit, were used in order to depict density distribution along the section, and to compare the distribution of the thermohaline properties with those observed by the CTs. Both θ and σ_0 are referred to the reference pressure at the sea surface.

3. Evidence of Eddies in the Time Series

[9] The subtidal currents were vertically homogeneous, at least within the portion of the water column covered by ADCP measurements (about 100 m thick), and highly variable with time [*Ursella et al.*, 2011]. The meridional current component (approximately parallel to the strait axis) prevailed over the zonal one and increased toward the bottom. Maximum mean values (−9.3 cm/s) were observed mainly at the central ADCP mooring (station V3), suggesting that V3 was positioned close to the core of the outflowing bottom flow. Mean current vectors were oriented southward (angle in the range from −52 to −148 degrees in the trigonometric system), with magnitudes between 5.5 and 11.35 cm/s. The principal axis analysis [*Preisendorfer*, 1988] of the subtidal flow shows that the currents close to the continental margin were strongly polarized along isobaths. Moving toward the center of the strait, the low-frequency motions became more circular. The major variance axes were parallel to the local orientation of isobaths, especially near the bottom.

[10] The entire section of the moorings was characterized by a pronounced pycnocline in the upper 50 m, by a gradual density increase in the interior and by a stratified bottom layer about 100 m thick in the center (as depicted by the November 2006 vertical density distribution in Figure 1c). The stratified bottom layer is the layer where the current profiles were measured. The low-shear vertical structure of the flow within this layer at the three moorings is well reproduced by the normal modes (a decomposition using a rigid-lid approximation). The first three baroclinic modes of the horizontal velocity display in-phase vertical variability and only the fourth and fifth modes indicate an out-of-phase structure within the current measurement layer. The deformation radii of the first and second modes were 6.3 and 3 km, respectively; they were ~1 km for the rest of the modes. The linear flat-bottom vertical modes and the corresponding radii of deformation were determined from the section-averaged buoyancy frequency profiles from the five CTD casts obtained during the November 2006 mooring deployment.

[11] Cross-correlations calculated between all pairs of current components [*Ursella et al.*, 2011] was high (>0.6) between the two extreme cells of each mooring. Generally, high negative correlation coefficients were between the

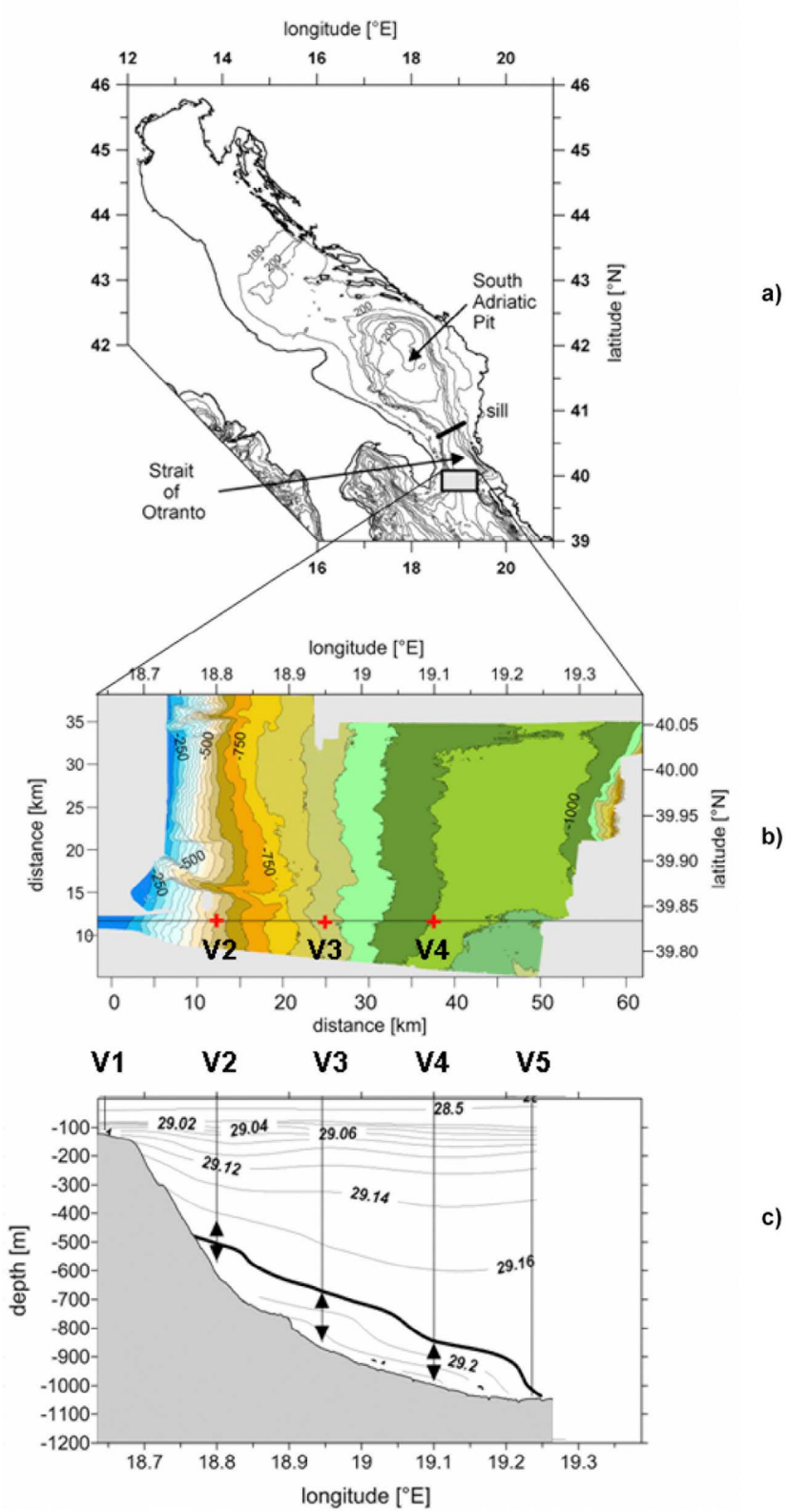

Figure 1. (a) The Adriatic Sea with 100, 200, 400, 600, 800, 1000, and 1200 m depth contours. (b) The shaded zone is expanded to show detailed bottom topography from the multibeam survey and location of moorings V2, V3, and V4 indicated by red crosses; (c) the sketch of the current meter moorings along the east–west section is superimposed on the density distribution in November 2006, obtained from the CTD casts at V1, V2, V3, V4, and V5. The uppermost and the lowermost ADCP cells are depicted with solid triangles. The thick line highlights the isopycnal 29.18 kg/m^3.

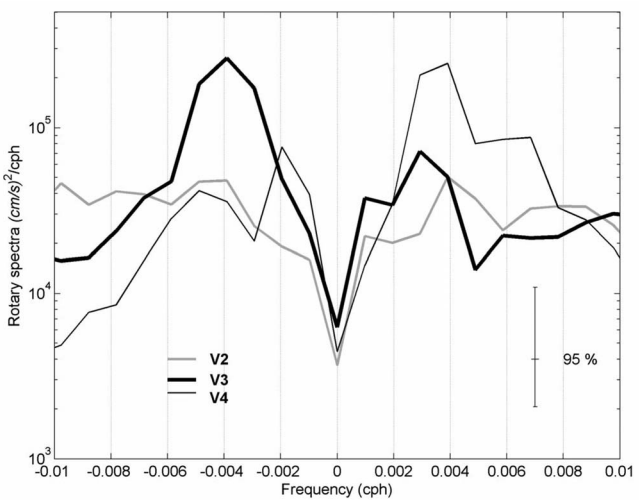

Figure 2. Rotary power spectra of current data from the deepest ADCP cell of each mooring, for frequencies lower than 0.01 cph (about 4 days): V2, (gray, 545 m depth), V3 (thick black, 825 m depth) and V4 (thin black, 963 m depth); 95% confidence level is indicated.

meridional components at stations V3 and V4 while for the same station pair the high positive correlation coefficients were between zonal components. This suggests current vector rotation in opposite senses at the two moorings. On the other hand, the correlation was positive, although of lower value, between moorings V2 and V3. This indicates that the two moorings were located on the same side of the passing eddies, as will be shown by the idealized eddy simulation and other observations.

[12] The rotary spectrum analysis applied to the data of the deepest ADCP cell, using windows of 4096 points with 2048 point overlap, confirmed the low-frequency rotation in opposite senses at V3 and V4, as obtained from the cross-correlation pattern. In fact, the rotary spectra (Figure 2) reveal a peak at a positive frequency of 0.004 cph (~10.5 day period) at the outer station V4, showing a prevalent counterclockwise rotation at this position. The peak also occurred at the central station V3 but at the corresponding negative frequency, indicating the presence of a signal on a timescale of about 10 days with a prevalent clockwise rotation. In contrast, the rotary spectra at the innermost station V2 did not show any statistically significant peak, and the variance distribution was generally symmetric around zero frequency.

[13] The dominant signal of an advected eddy at a single mooring is expected to appear in the component normal to the advection velocity [*Lilly and Rhines*, 2002], with initially positive (negative) values for a cyclone (anticyclone). Due to the general north–south alignment of the velocities, the *u* component can be considered approximately perpendicular to the advecting flow. The *u* component is represented in Figure 3 for V2, V3 and V4, for the whole period of measurement. The significant events are identified in Figure 3 by a change in the *u* component of about 20–30 cm/s. Many of

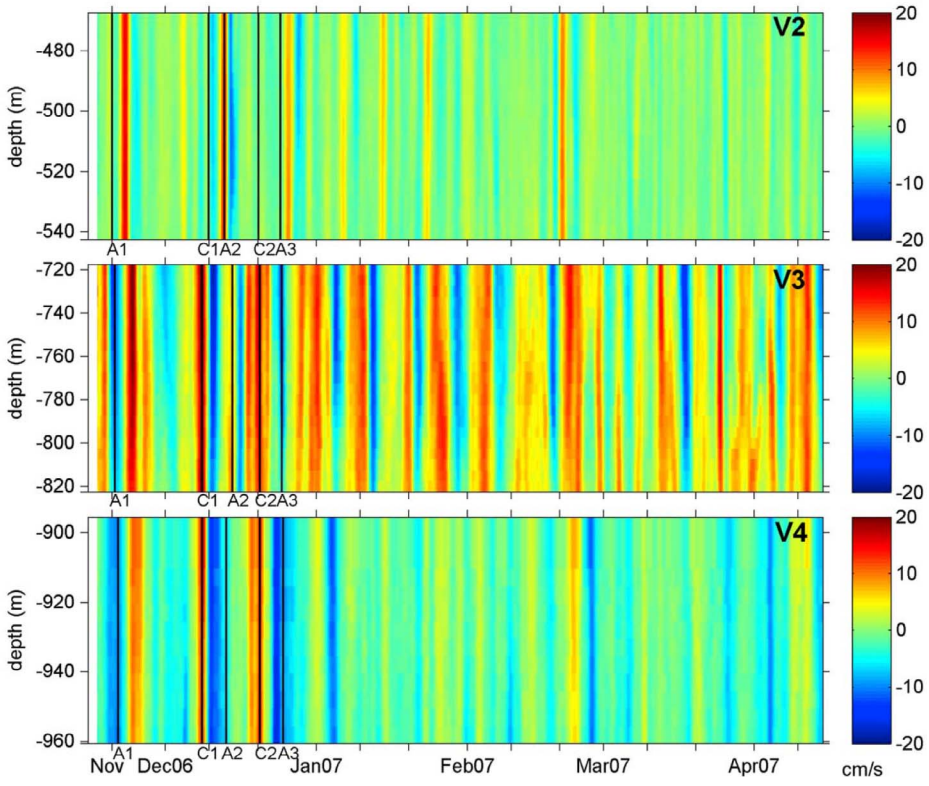

Figure 3. Time evolution of the *u* component (approximately coincident with the across-advection component) along the vertical, for the whole period, for stations V2, V3, and V4. The depth-averaged initial time of each rotational event is indicated by a line.

them were observed at station V3 during the whole measurement period, while stations V2 and V4 showed the most significant events confined to the first part of the measurement period. Therefore we concentrate our analysis on five events identified in November–December 2006: two of them were cyclones (C1, between 7 and 11 December, and C2, between 20 and 24 December 2006) and their signal was very clear at the two deeper stations V3 and V4 (initially positive u-current component); the other three were anticyclones: the event A1 (20–24 November) was present at all three stations while events A2 (13–16 December) and event A3 (24–28 December) were seen predominantly at the shallower stations V2 and V3. A weaker event was also evident at the end of February 2007 at the three stations, but it is not discussed in detail in this paper. The slightly different timing of the same event at the three stations is caused by a difference in the arrival of the eddy at the locations due to its shape. In Figure 3 the depth averaged initial time of each event, as obtained from the analysis detailed in section 5, is indicated by a line.

[14] On the hodograph planes, eddies are expected to appear as D-shaped structures (unlike fronts or filaments which result in straight lines) and to result in a straight line when sliced through their exact center [*Lilly and Rhines*, 2002]. In this last case, eddies can be distinguished from fronts using additional information, such as current component behavior and rotation in the progressive and stick diagrams. In addition, the hodographs permit to understand if the eddy core passes over the mooring position, and if that mooring is more affected than the others. In accordance with these theoretical points, the hodographs (not shown) for the first measurement period at the two stations V3 and V4 display five and three D-shaped structures, respectively, in correspondence with the events. In particular, event C1 was very clear and present as a semicircular shape at V4 and an almost straight line at V3 (Figure 8).

[15] In order to better illustrate these rotational events in the time domain, the progressive vector diagram of currents at the three stations together with density are presented in Figure 4a. It is evident that density is higher for cyclones (triangles at the central time) than for anticyclones (circles at the central time), and that the cyclonic events tended to be cooler than the anticyclonic ones (not shown).

3.1. Cyclonic Events

[16] The two major cyclonic events at stations V3 and V4, C1 and C2, are evidenced in Figure 4a by red triangles at the central eddy time. From the time series for moorings V3 and V4 (Figure 4b), prominent out-of-phase variations in the v component are present. In contrast, the u components are in phase. Calculating the horizontal shear of both velocity components along the east–west direction (not shown), two major positive peaks are seen for the v component between stations V3 and V4, in connection with events C1 and C2. They are due to the fact that the v component at two stations is out of phase. The positive peaks in the shear of the v component are in agreement with the passage of cyclones traveling southward and with their center between the two stations.

[17] The footprint of mesoscale eddies is also evident in both CT (Figure 4a, for density only) and turbidity records (Figure 4c). A detailed look into the C1 and C2 events, when eddy passage is presumed, shows a number of coincidences: eastward velocity at V3 and V4 was maximum (Figure 4b), turbidity rose at V4 (Figure 4c), and temperature and salinity dropped at V3 and V4 (as it will be shown in detail in section 6). More precisely, the turbidity maximum occurred at the beginning of the rotational event, when the currents were directed from the continental slope toward the center of the Strait and were rather strong (up to 20 cm/s). As soon as the current turned southward the turbidity reduced to background levels.

[18] Once the average current has been eliminated from time series, these events appear as rotational motions with convergent vectors (Figure 5). The flows at locations V3 and V4 along the north–south axis were in opposite directions for most of the time. From these diagrams it is also evident that the clockwise rotation at V3 coincided with the counterclockwise rotation at V4. Such events in the time series actually determine a dominant pattern of opposite rotation on a 10 day time scale; this has already been seen from both rotary spectra (Figure 2) and the cross-correlation coefficients. During these two events, the flow at the mooring V2 was southward, that is, in phase with V3 and out of phase with V4.

[19] In an attempt to explain these coincidences, the presence of the following phenomena are suggested: the cross-shore bottom flow from the western shelf down the canyon (Figure 1b) to the abyssal depths causes the increased sediment transport recorded at least up to V4 (turbidity increase, eastward velocity maximum). The canyon, located upstream of the measurement transect and almost parallel to it, probably represents a conduit for the cross-shore water transport toward the center of the strait. Mooring V2 was located at shallower depths and to the west of the mouth of the canyon, and therefore cannot be influenced by any flow descending the canyon.

3.2. Anticyclonic Events

[20] The three anticyclonic events A1, A2 and A3 were weaker in current intensities than cyclones. Event A2 was particularly intense at station V2, but it is difficult to clearly identify it as an anticyclone through the analysis exposed in chapter 5. This is probably due to the interference with event C1.

[21] Anticyclones were practically the only episodes during the whole measurement period for which the v component consistently reversed to positive values at V3 (Figure 4b). Positive values for the v component were also observed at V2, while negative ones were registered at V4. Therefore, the v component at V2 and V3 was in phase while it was out of phase at V3 and V4. This suggests the passage of the eddy center between stations V3 and V4.

[22] For anticyclonic eddies (Figure 4a) density decreased at the three stations; eastward and northward velocities at V2 were positive and maximum, while temperature and salinity increased, as it will be shown in section 6. There was no change in the turbidity, probably due to lower velocities which were not able to resuspend and/or advect particles.

[23] Contrary to the situation with cyclones, these events appeared as rotational motions with divergent vectors (Figure 5). The flows at locations V3 and V4 along the north–south axis were in opposite directions for most of the time. From progressive diagrams (Figure 4a) it is also evi-

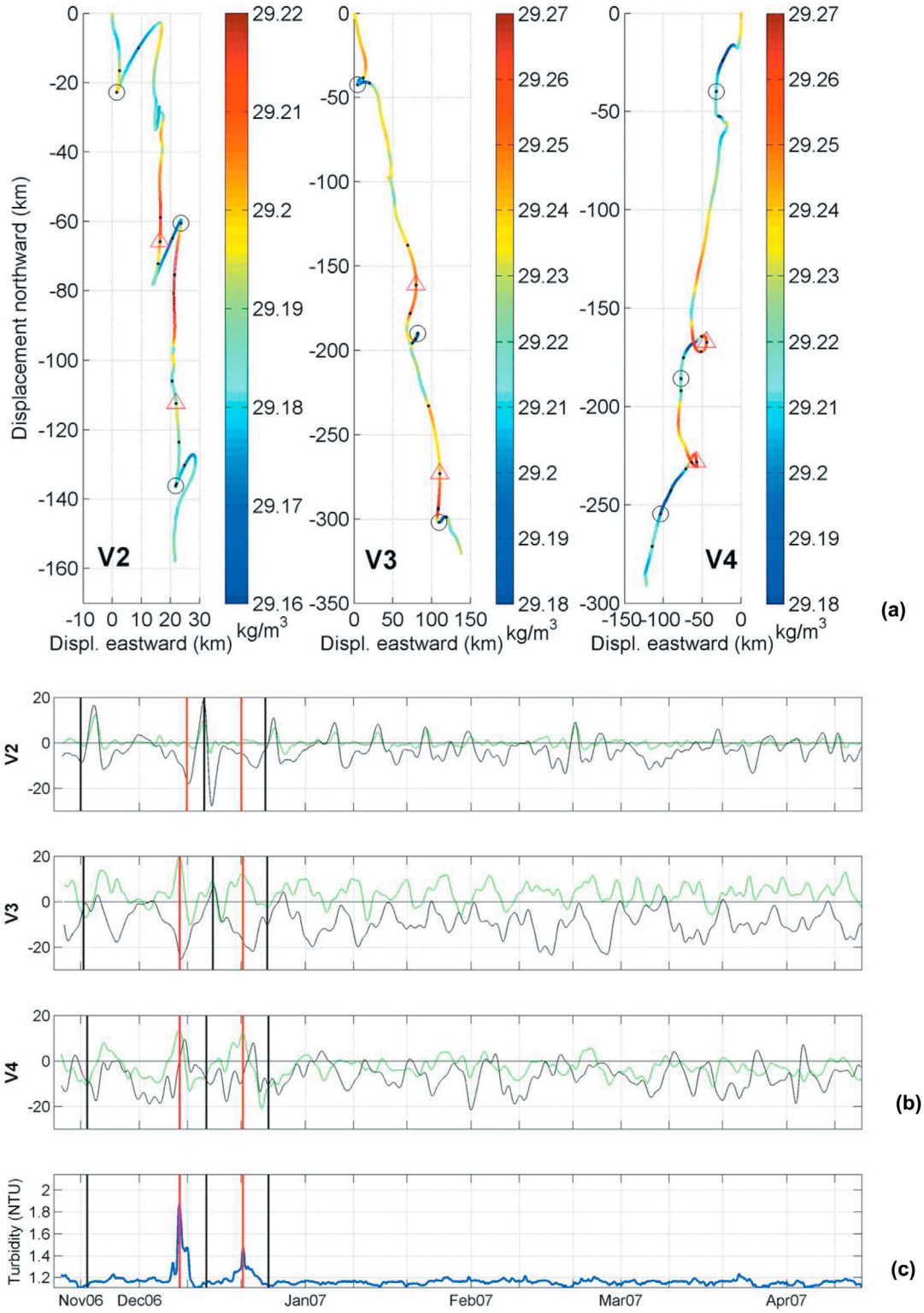

Figure 4. Events at the deepest level at the three stations: (a) progressive vector diagram for the first measurement period (until the end of December 2006); colors represent density; the cyclonic and anticyclonic events are indicated by red triangles and black circles, respectively; the center of the symbols corresponds to the central time of each event. (b) The *u* (green) and *v* (black) current components at stations V2, V3, and V4. The initial times of the cyclonic and anticyclonic events are indicated by red and black lines, respectively. (c) Turbidity time series at station V4.

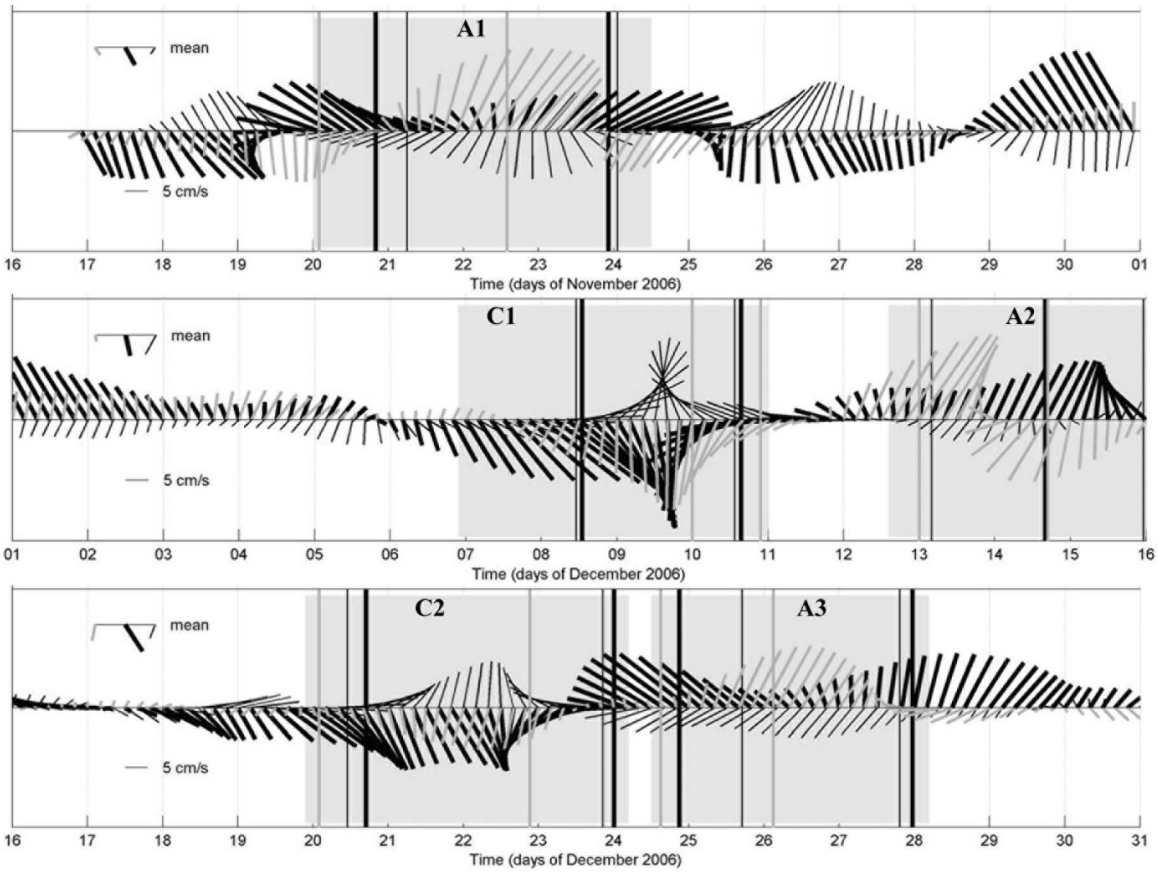

Figure 5. Stick diagram of currents at the deepest ADCP cell during the period 16 November through 31 December 2006: V2 is gray, V3 is thick black, and V4 is thin black. The mean over the indicated period is plotted for each current meter in the left upper corner, and it has been removed from each time series. Each event is indicated with vertical lines (the start and the end times for the deepest cell) of the same color as the corresponding station's vectors. Shaded areas indicate the overall eddy duration.

dent that the clockwise rotation at V2 and V3 coincided with the counterclockwise rotation at V4.

4. Idealized Circular Eddy Footprint

[24] In order to verify whether the rotational events can be associated with simultaneous mesoscale eddy passages at the three moorings, we analyzed the effect of an idealized, rigid, circular and symmetric eddy on Eulerian current records. We considered a simple model of cyclonic and anticyclonic eddies that consist of a solid-body rotation within a core, with the tangential velocity linearly increasing with the radius. The azimuthal speed is maximum at the edge and then decays as the inverse of the distance from the core [*Lilly and Rhines*, 2002]. In this idealized case three measurement points, V2, V3 and V4, were considered, as in our field experiment, assuming that the eddy core radius is 15 km, which is slightly larger than the V3–V4 mooring distance. Peak azimuthal speed at the eddy edge was chosen to be 25 cm/sec. Considering that isobaths are not perpendicular to the mooring transect and that eddies are expected to travel almost parallel to them, they were assumed to propagate along a trajectory with an angle of about 25° clockwise from north. The advection speed of idealized eddies was chosen to be 15 cm/sec, which is close to the mean velocity obtained from current meters. The case resulting in the greatest similarity between the idealized and the measured signal is the one associated with the southwestward propagation of either cyclonic or anticyclonic eddies, as demonstrated in Figure 6. Therefore, events of counterclockwise (clockwise) rotation at station V4 (V3) could be linked to passages of cyclonic eddies in the southwestward direction. The same applies to anticyclonic eddies except that cyclonic eddies produce convergent currents while anticyclonic ones show resultant vectors that have divergent temporal behavior. Also, the passage of cyclonic eddies generates a northward meridional current component to the left of the eddy center and southward meridional current component to the right of it, looking in the direction of eddy propagation. The passage of anticyclonic eddies gives the opposite direction of meridional current components. The idealized case demonstrates that eddies of the dimension of 30 km diameter also show a signal at mooring V2 as observed from experimental data. Finally, the eddy dimensions and the location of the eddy center trajectory with respect to the position of V2, V3 and

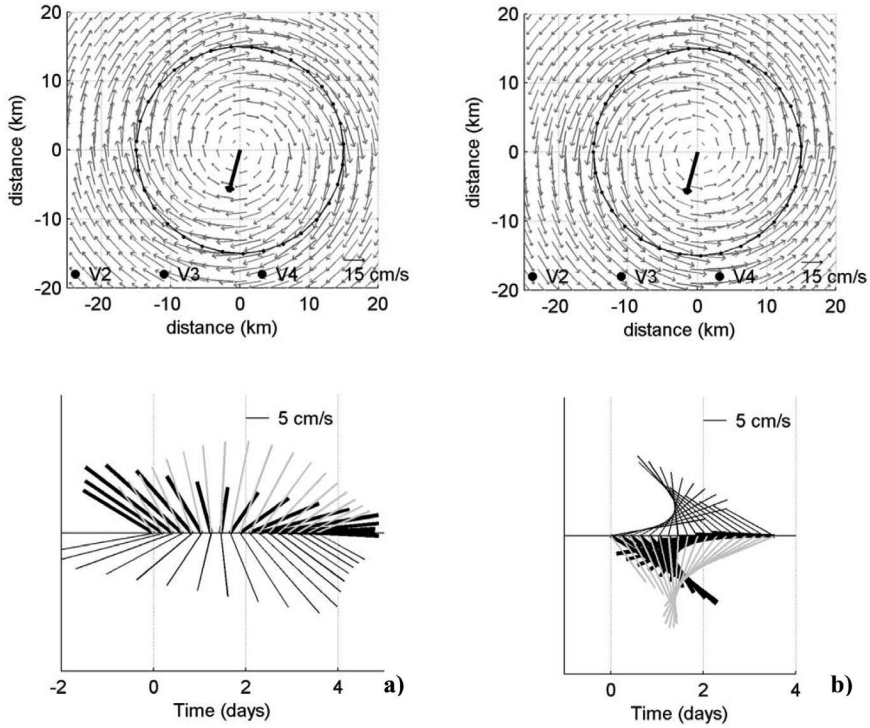

Figure 6. Idealized rigid circular (a) anticyclonic and (b) cyclonic eddies passing over the mooring locations. (top) Measurement sites are indicated by dots. The black circle delimits the eddy core, whose peak azimuthal speed is 25 cm/s. Grey arrows represent the velocity field generated by the eddy. The advection velocity (15 cm/sec) is depicted by an arrow at the eddy center. (bottom) The obtained stick diagrams at the three moorings: V2 is gray, V3 is thick black, and V4 is thin black.

V4 determine the prominence of the rotational episodes at the stations and the correlation between different moorings.

5. Eddy Parameters

5.1. Mean Values

[25] Following *Lilly and Rhines* [2002], estimations of some characteristic eddy parameters were made. Specifically: t_0 is the time at which mooring enters the eddy core; Δt is the time in days of "permanence" inside the core; V is the peak azimuthal eddy velocity at any depth; and the advection velocity, defined by a speed (Uadv) and a direction (Θ), is the velocity of propagation of the eddy. Δt, t_0 and V are calculated maximizing the velocity difference over a window in the time series around an initial guess for the time t_0. The best estimate of V with this method is obtained when the eddy center passes over the mooring. As the velocity in the direction perpendicular to the advection velocity is expected to be largest, the advection direction can be estimated from the direction of V plus $\pi/2$. A second estimate for V can be obtained by subtracting an estimate of the advecting flow from the velocity at the core edge. Two methods were used to estimate the velocity of advection at the eddy center; the first one ($Uadv_a$ and Θ_a) minimizes the angle difference between the observed currents minus an estimate of the advection velocity, and the observed vertical shear (independent of the advection velocity); the second one ($Uadv_f$ and Θ_f) uses a low-pass filter, with a hanning function whose length is 4 × the eddy duration, to get the advection velocity at the eddy central time. This second method is useful when advection velocity is large with respect to the eddy velocities and is slowly varying relative to eddy duration. The two methods give comparable estimations of velocity of advection Uadv in most of the cases. They are used to determine the eddy chords as X = Δt *Uadv, i.e., the length in km corresponding to the time interval Δt for which the mooring is crossed by the eddy core. Two different values for chords are therefore obtained from each mooring for each event; the discrepancy between the two indicates an irregular spatial structure and shape of the eddies. Rossby number is also calculated as V/(X*f). The estimates of these parameters are reported for each event in Table 1. Because slightly different values for the parameters were found at each ADCP cell, all quantities given in Table 1 are averaged over depth. As already mentioned, event A2 is difficult to exactly determine and therefore its parameters are more uncertain than for others events. Moreover, in the case of event A2 and A3, no values for chords are given, due to the fact that the moorings are not located within the eddy core, but just outside of it. In this case, also t_0 and Δt attain a different meaning, i.e., the interval for which the mooring is influenced by the eddy field.

[26] Looking in detail at the eddy parameters, and considering here just the two stations principally involved by each of the eddies, it is evident that eddy peak azimuthal velocity was always between 12 and 21 cm/s; advection velocity was always below 15 cm/s, with direction in the third and fourth trigonometric quadrants; the Rossby number was between 0.03 and 0.6, with just one case being greater than 1 (1.13 during event A2 at station V2). Small

Table 1. Eddy Parameters Averaged Over Depth[a]

	A1			C1			A2			C2			A3		
	V2	V3	V4	V2	V3	V4	V2	V3	V4	V2	V3	V4	V2	V3	V4
t_0	20/11 0	20/11 13	21/11 5	09/12 22	08/12 12	08/12 12	13/12 3	14/12 18	13/12 12	20/12 1	20/12 8	20/12 8	24/12 13	24/12 21	25/12 3
Δt (days)	2.6	3.7	3.1	0.9	2.3	1.9	1.5	1.9	2.5	2.6	4.6	3.4	1.6	3.8	2.9
$Uadv_a$(cm/s)	4.0	8.0	10.5	12.0	5.2	6.1	7.1	2.1	12.4	5.8	11.8	1.3	3.4	6.2	1.6
Θ_a (degrees)	34	−69	−99	−120	−114	−156	−154	−63	−101	−88	−100	−145	74	−33	−147
$Uadv_f$(cm/s)	2.4	6.9	2.8	11.7	14.7	2.8	1.6	3.3	4.6	5.4	8.9	2.9	1.4	7.2	7.3
Θ_f (degrees)	−46	−57	−111	−101	−81	−129	−88	−52	−111	−94	−66	−113	−61	−61	−138
V_n (cm/s)	16.6	14.6	10.7	5.9	18.0	13.5	22.6	12.1	5.2	4.4	15.2	14.9	8.6	10.3	2.7
V_u (cm/s)	17.0–16.9	17.3–16.3	13.3–10.7	6.6–6.9	18.0–20.8	13.4–13.5	23.5–22.6	12.1–12.3	8.6–5.2	4.5–4.4	15.6–15.1	15.4–15.0	8.7–9.7	12.0–13.3	8.5–3.6
Rossby number	0.21–0.33	0.07–0.08	0.05–0.15	0.08–0.08	0.22–0.07	0.14–0.31	0.27–1.13	0.38–0.25	0.03–0.05	0.04–0.04	0.04–0.05	0.43–0.19	0.20–0.49	0.06–0.06	0.22–0.02
X_a (km)	8.8	25.5	28.4	9.0	10.3	10.1	9.4	3.4	n.s.	12.8	46.3	13.8	4.7	20.3	n.s.
X_f (km)	5.4	22.1	7.5	8.8	29.4	4.6	2.1	5.4	n.s.	12.0	34.9	8.7	1.9	23.6	n.s.
θ (°C)	13.594 ± 0.032	13.500 ± 0.055	13.503 ± 0.047	13.565 ± 0.017	13.234 ± 0.022	13.217 ± 0.047	13.617 ± 0.083	13.494 ± 0.105	13.468 ± 0.033	13.620 ± 0.021	13.256 ± 0.047	13.206 ± 0.096	13.615 ± 0.033	13.418 ± 0.158	13.555 ± 0.032
S	38.768 ± 0.003	38.760 ± 0.004	38.765 ± 0.005	38.776 ± 0.006	38.743 ± 0.002	38.742 ± 0.005	38.774 ± 0.002	38.760 ± 0.004	38.770 ± 0.006	38.773 ± 0.002	38.746 ± 0.004	38.743 ± 0.007	38.761 ± 0.006	38.756 ± 0.011	38.759 ± 0.006
σ_0 (kg/m^3)	29.191 ± 0.009	29.204 ± 0.012	29.208 ± 0.011	29.203 ± 0.007	29.248 ± 0.004	29.251 ± 0.006	29.191 ± 0.018	29.206 ± 0.012	29.219 ± 0.002	29.189 ± 0.004	29.245 ± 0.007	29.253 ± 0.015	29.181 ± 0.003	29.219 ± 0.028	29.192 ± 0.011

[a]The initial time of eddy passage at the mooring is given by t_0; Δt is the temporal eddy duration, X is the eddy chord intersected by the mooring, Uadv is the average over depth of advection speed, and Θ is the mean advection speed angle. Subscript "a" stands for angle method, while subscript "f" stands for filtering method. V is the estimated edge eddy current (Vn was calculated maximizing current meter velocity-time differences, while Vu was obtained by subtracting from velocities an estimate of the advecting flow). Two values are given for Vu and the Rossby number, due to two different estimates of the advection velocity. For details on quantities and calculation methods, see *Lilly and Rhines* [2002]. Mean and standard deviation of potential temperature (θ, °C), salinity (S), and potential density (σ_0, kg/m^3) are also indicated; n.s., not significant.

Rossby number means that Coriolis force prevails over the inertial terms and the flow can be considered linear. It is evident from Table 1 that the arrival time at the three stations was not exactly the same, probably due to the almost circular shape of the eddy, whose border reached the moorings positioned along a line at different times.

[27] In order to obtain values for the distance of mooring from eddy center (r) and the eddy radius (R) (Table 2), geometrical considerations based on a cylindrical eddy passing at two of the three moorings (Figure 7) were used. Accordingly, for each of the events the two stations typically affected by the eddy were used in the calculation of these parameters. Moreover, a unique value for the eddy advection velocity at the two moorings is needed and the average value between the advection velocities at the two locations was calculated. The advection velocity used at this scope is generally $Uadv_f$, because it is directly calculated from time series; however, when the obtained value is too small (as for A2 event) and therefore the calculation method is not justified, the $Uadv_a$ is utilized. Cyclonic and anticyclonic eddies have radii between 10 and 18 km, and cyclonic events seem to be bigger. Station V3 was close to the eddy center (within 3 km) for all the events except for A2. For events C1 and C2 (cyclonic ones) the eddy center passed very close to mooring V3, and in fact the length of the intersected chord is close to the eddy diameter. Generally, cyclones travel faster and occupy larger depths than anticyclones.

5.2. Comparison Between Real and Theoretical Events

[28] In order to experimentally verify the theory of *Lilly and Rhines* [2002], theoretical current behavior is compared to experimental data in the case of event C1 (Figure 8). The parameters used to run the eddy model (Figure 8a) are the advection velocity, eddy radius and position of moorings with respect to eddy center for the event C1 (as reported in Table 1), while the peak azimuthal speed is taken from station V3 (Table 2), which gives the best estimate, as V3 slices the eddy through its center. It is interesting to note that chords (Figure 8a), event duration and the stick diagram (Figure 8b) coming from the model are completely comparable with the ones obtained from data and single mooring calculations (see Table 1). For what concerns the real hodographs (Figure 8c), they are plotted for an interval larger than the eddy core passage. The linear part of the theoretical hodograph refers to times inside the eddy core. There is a good accordance between the real and ideal hodographs, in particular as far as the stations V3 and V4 are concerned. Figure 8d indicates that the *u* component from the experimental data at V3 and V4

Table 2. Advection Speed (Uadv), Advection Direction (Θadv), Eddy Chord (X), Distance of Mooring From the Eddy Center (r) for Each of the Two Indicated Stations and Eddy Radius (R), as Deduced From Two Moorings Geometrical Considerations[a]

	A1 V3/V4	C1 V3/V4	A2 V2/V3	C2 V3/V4	A3 V2/V3
Uadv (cm/s)	4.9	8.8	4.6	5.9	4.3
Θadv (degrees)	−84	−105	−108	−90	−61
X (km)	22.1/7.5	29.4/4.6	9.4/3.4	34.9/8.7	1.9/23.6
r (km)	3.2/10.9	−0.84/14.5	5.3/6.9	−3.0/17.2	11.8/0.6
R (km)	11.5	14.7	7.1	17.7	11.8

[a]See text for details.

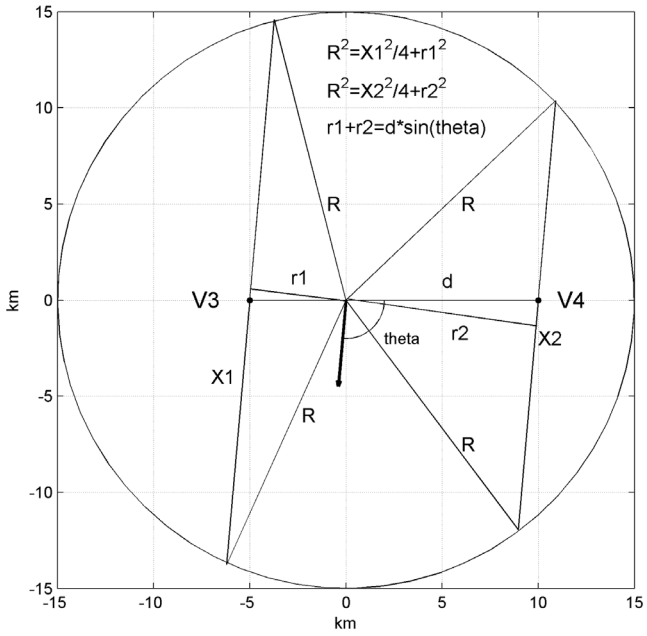

Figure 7. Geometry from which eddy radius (R) and mooring distances from eddy center (r1 and r2) are obtained. X1 and X2 are the chords intersected by the moorings V3 and V4, as obtained from a single mooring's calculations; *d* is the distance between moorings; theta is the advection velocity angle in the trigonometric system. Advection velocity is indicated by an arrow in the eddy center.

reverses during the eddy passage, whereas the *v* component maintains its sign, which is opposite at the two stations; their temporal variations are very similar to the theoretical results, shown by *Lilly and Rhines* [2002, Figure 7]. Moreover, the availability of current records from the three moorings during the passage of eddies, permits to verify for the first time the validity of the technique proposed by *Lilly and Rhines* [2002].

5.3. Vertical Structure

[29] The characterization of eddies was performed using mean values of all quantities over the portion of the water column covered by the measurements. These parameters, however, show some weak vertical dependence. As event C1 is the one for which the eddy was sliced exactly at its center by mooring V3, we will discuss in the following the vertical structure of its characterizing parameters (Figure 9). It is clear that parameters, calculated as described in paragraph 5.1, do not change very much along the vertical. So, initial times and duration (Figure 9a) vary within a few hours from the top cell to the bottom one; eddy peak azimuthal velocity (Figure 9b) are within 4 cm/s; advection velocity components (Figure 9d) vary within few cm/s; eddy chords (Figure 9e) within 5 km; Rossby number (Figure 9f) is within 0.02 units. The velocity across the direction of advection (Figure 9c) displays a steeper slope during the eddy passage, just between its initial and end times. Comparing the values of these parameters at different stations, eddy peak azimuthal velocities are between 13 and 22.5 cm/s. Advection velocity increases slightly toward the bottom, attaining maximum values (about 15 cm/s) at V3. The chords present their maximum values at station V3, decreasing toward the bottom due to the decreasing event duration. Finally, the Rossby number decreases with depth at the three stations, with the smallest values (between 0.059 and 0.072) at the central station.

6. General Thermohaline Properties and Their Characteristics During the Five Rotational Events

[30] The time series of the thermohaline properties from the CTs above the seabed at the three moorings were used to characterize both the typical and the eddy characteristics.

6.1. Typical Thermohaline Properties in the Bottom Layer

[31] As mentioned before, the bottom layers of the V3 and V4 are characterized by the AdDW outflow and by a stronger vertical gradient of density (Figure 1c). The AdDW is delimited by an isopycnal of 29.18 kg/m^3 [*Manca et al.*, 2003]. Its density is thus generally higher than 29.18 and lower than 29.3. The time average values of the entire θ, S, and σ_0 series coupled with the corresponding standard deviations (Table 3) can be regarded as typical values of the AdDW outflowing vein in the bottom layers for the period of study. Generally, θ and S were lower, and σ_0 higher at V3 and V4, and vice versa at V2. This is coherent with the location of V3 and V4 within the core of the fresher, cooler and denser AdDW. The range (maximum-minimum) of θ, S, and σ_0 values (Table 3) was larger at V3 and V4, and smaller at V2. The same also holds for the variances (standard deviations) of θ and σ_0.

[32] The moored CTs (19 m above the seabed) captured two types of signals: the one of denser waters that is not observed by the CTD cast, and the other of the lighter waters, that according to the CTD casts reside at intermediate depths above the mooring area.

[33] Densities larger than 29.3 occasionally observed in the bottom layers of the Strait, are found in the Southern Adriatic Pit where the AdDW has its origin [*Manca et al.*, 2002]. This is corroborated here from the CTD casts performed in both regions, and illustrated by the θ-S diagram in Figure 10a.

[34] The intermediate layers above the AdDW at the Otranto section and in the Southern Adriatic Pit are distinguished by their higher S and θ (Figure 10a). Subsurface S and θ reach their maximum at approximately 200 m depth (at the density horizon between 29 and 29.15 kg/m^3; see Figure 10a) being signatures of the intermediate waters originating in the Levantine/Aegean basins [*Manca et al.*, 2003]. They inflow along the eastern flank in the Strait, spread toward north, and partly recirculate in the SAP.

6.2. Eddy Thermohaline Properties in the Bottom Layer

[35] The start and the end of the events at the lowest ADCP cell determined the time interval within which the respective mean thermohaline properties were calculated. The statistical characteristics of θ, S and σ_0 associated with each eddy are represented in Table 1. The mean θ and S values are depicted in Figure 10b. It is evident that the θ-S drop during the cyclonic events (C1 and C2) and θ-S increase during the anticyclonic events (A1, A2 and A3) were coherent at V3 and V4, as shown in Figure 10b. In

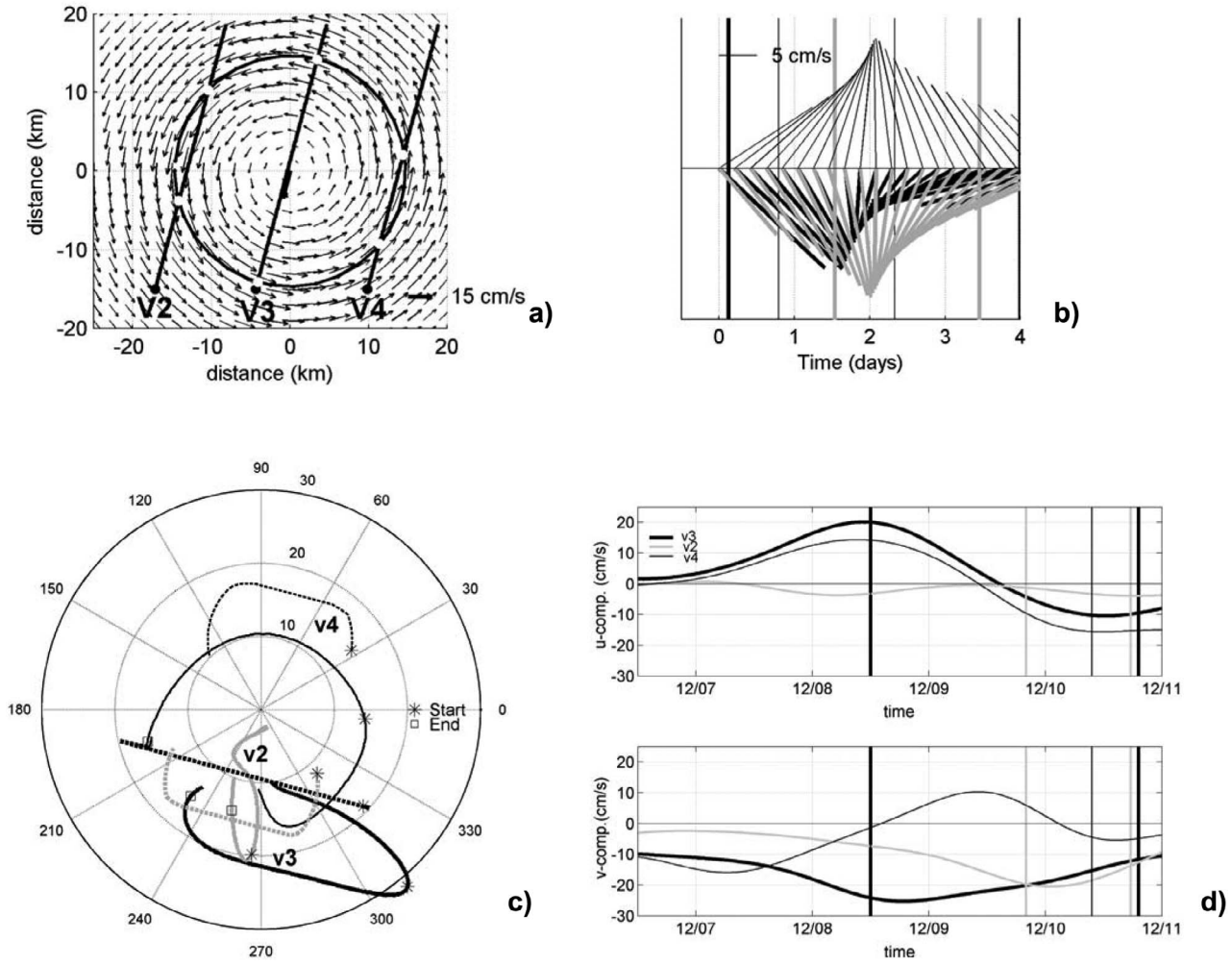

Figure 8. (a) Idealized eddy model set up with the parameters for event C1 contained in Table 2 (white dots delimit the chords at each mooring) and (b) the resulting stick diagram in which the start and end time of the event, corresponding to the white dots in Figure 8a, are indicated with lines of the same color as the vectors. (c) Hodograph, with solid lines indicating real data and dotted lines representing the theoretical ones, as obtained from model in Figure 8a. (d) Current components from time series. The colors of the lines are consistent within all the panels: gray for V2, thick black for V3, and thin black for V4.

particular, the θ-S properties tended to group at the two opposite sides of the θ-S diagram: cyclonic at the higher densities, with lower θ and lower S, and anticyclonic at lower densities, with higher θ and higher S. In other words, at V3 and V4, cyclonic events are characterized by θ and S lower, and σ_0 higher, than the typical AdDW outflow, while the anticyclonic events are characterized by θ and S higher, and σ_0 lower, than the typical AdDW. Such differences between the cyclonic and anticyclonic events were not observed at V2. When compared to the characteristics of the overflow in the Denmark Strait [*Spall and Price*, 1998] our case shows the presence of not only cyclonic but also anticyclonic eddies just inside the AdDW overflow, while in the Denmark Strait only cyclonic eddies are evident. In addition, the Denmark Strait cyclonic eddies bear the signature of the lighter intermediate waters, while in our case the cyclonic eddies well up denser waters, and anticyclonic ones imbed lighter waters.

[36] The passage of the cyclonic events over locations of V3 and V4 was associated with upward displacement of the isopycnals (convex shape, higher density at the level of the CT sensors). Conversely, the passage of the anticyclonic events was accompanied by downward displacement of the isopycnals (concave shape, lower densities at the level of the CT sensors). The latter case is confirmed when comparing the θ-S properties at V3 and V4 during the three anticyclonic events with those characterizing the layers situated about 100 m above (corresponding to the density horizon of about 29.19–29.20 kg/m^3 in Figure 1c).

[37] The density values recorded during the two cyclonic events in December 2006 at V3 and V4, as well as maximum density recorded by the CTs, are higher than those captured by the CTD measurements at about 10 m above the seabed at the same locations in mid November 2006 and in mid April 2007 (Figure 10b). The fact that CTs occasionally recorded higher density values indicates that the very bot-

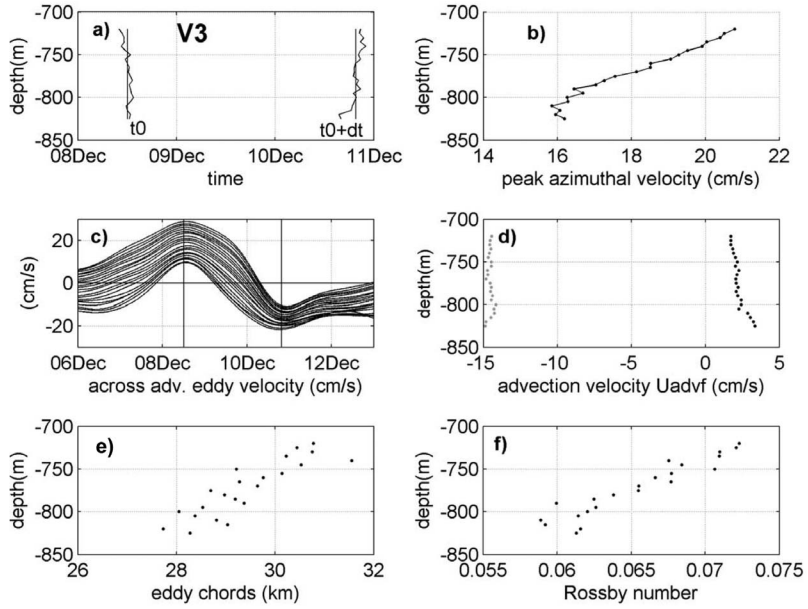

Figure 9. Vertical structure of eddy parameters at station V3 for event C1: (a) initial time (t_0) and end time ($t_0 + \Delta t$); (b) eddy peak azimuthal velocity V_n (cm/s); (c) time series of a cross-advection eddy velocity (cm/s): the upper curve corresponds to the top cell, and the other curves are shifted by 1 cm/s each; note that the time scale has a wider range than for Figure 9a); (d) $Uadv_f$ advection velocity components (gray, north comp.; black, east comp.); (e) eddy chord X_f (km); (f) Rossby number.

tom layers of the Otranto section are periodically (at timescales of about 10 days) flushed by the denser waters that usually reside to the north, in the Southern Adriatic Pit (Figure 10a). For that reason, in addition to the isopycnal upward displacement that increases the density at the CT levels, the cyclones may entrap the denser portion of the AdDW overflowing the sill. These pulsations leave distinct signals in the center of the Otranto section. Conversely, the anticyclones trap lighter intermediate waters and push them toward the seabed in the center of the section.

[38] At V2, θ variations associated with the five examined rotational events were smaller than at V3 and V4 while S variations were similar to those at V3 and V4 (Table 1 and Figure 10b). A combination of observed θ-S properties at V2, however, did not allow the distinction between the cyclonic and the anticyclonic eddies as clearly as at V3 and V4 for the five cases. This is due to its location over the slope, in a region with smaller vertical density gradients (as well as of θ-S) and out of the AdDW outflow core (Figure 1c).

7. Discussion and Conclusions

[39] The results of our analysis of the current meter records from the period November 2006 through April 2007 along the western portion of the Strait of Otranto show prominent rotational episodes of current vectors with a vertically homogeneous structure within the measurement depth range of about 100 m above the seabed.

[40] Similar rotational events were noticed in the current time series collected in the period 1997–1999 [*Manca et al.*, 2002, *Ursella et al.*, 2007] at the same current meter mooring network. They were particularly strong in winter-spring 1999 and weaker during winter-spring 1998. It is documented that winter-spring 1999 was characterized by strong deep convection in the southern Adriatic, with production of a great amount of AdDW and increased outflow from the Adriatic [*Manca et al.*, 2002]. Conversely, during winter 1998 a weaker dense water outflow occurred due to less intense deep convection. The events of autumn 2006 are comparable in strength (i.e., comparable rotational velocities) with those of April 1999. The presence of the strong episodes in particular periods of the year seems to be related to the maxima in the outflow from the Adriatic Sea. The Adriatic Dense Water reservoir is filled up with the newly formed water only by the end of winter and thus the outflow from the Adriatic reaches its maximum after the convection season, i.e., in April/May. On the other hand, the rotational events during autumn seem to be related to a maximum of the water exchange Adriatic/Ionian water exchange that takes

Table 3. Typical Thermohaline Properties of the AdDW Vein Near the Bottom of the Strait of Otranto[a]

	V2	V3	V4
Δt (days)	149.6	149.8	150
θ_avg ± θ_std	13.636 ± 0.045	13.353 ± 0.093	13.432 ± 0.115
θ_min-max	13.496–13.794	13.123–13.600	13.129–13.609
S_avg ± S_std	38.771 ± 0.005	38.760 ± 0.004	38.765 ± 0.005
S_min-max	38.756–38.790	38.735–38.781	38.735–38.783
σ_0_avg ± _σ_0_std	29.184 ± 0.009	29.231 ± 0.014	29.218 ± 0.020
σ_0_min-max	29.164–29.221	29.175–29.265	29.172–29.265

[a]Time average (avg), standard deviation (std), minimum (min) and maximum (max) values of potential temperature (θ, °C), salinity (S), and potential density (σ_0, kg/m^3), calculated from the low-passed, hourly sampled CT data time series. Starting time is on 16 November 2006; duration Δt (days) at each station is indicated.

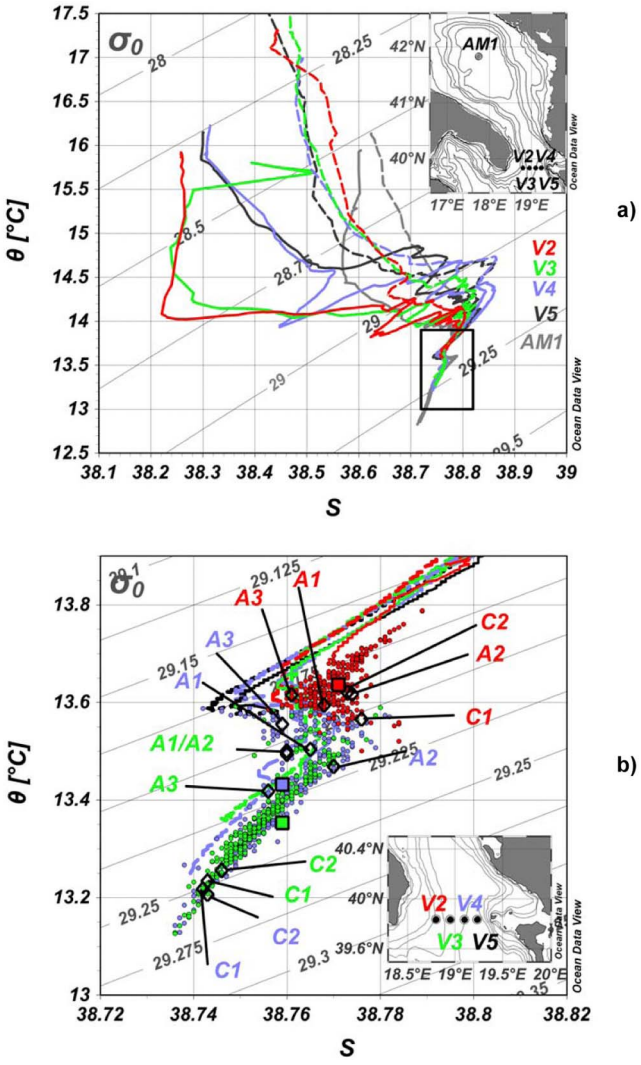

Figure 10. θ/S diagram: (a) CTD casts conducted in the Strait of Otranto at stations V2, V3, V4, and V5, and in the Southern Adriatic Pit at AM1 (see the inset map). November 2006 and April 2007 profiles are indicated by colored dashed and solid lines, respectively. The heavy rectangle delimits the layer below 450 m, which is expanded in Figure 10b for the Strait of Otranto; (b) CTD casts at stations V2, V3, V4, and V5 as in Figure 10a, superimposed to the CT time series at V2, V3, and V4 subsampled twice a day (color coded dots). Large squares correspond to the overall time average θ and S at V2, V3, and V4, while large diamonds correspond to the time-averaged eddy values (from Table 3). Mean values are from Table 3. C1 and C2 denote cyclonic events, while A1, A2, and A3 indicate anticyclonic events. At V3 and V4, events C1 and C2 cluster at lower θ and S (larger σ_0), while events A1, A2, and A3 group at higher θ and S (lower σ_0). The two types of events are not so well distinctive at V2.

place typically in late autumn (November/December). Thus, interannual variability in the rotational events is mainly due to the variations of the strength of the vertical convection and to the water exchange through the Strait of Otranto in general.

[41] Our analysis shows that the variability timescale related to the events was approximately 10 days. Cross-correlation and rotary spectral analysis of current time series revealed occurrence of the counterrotating events at the outermost and central moorings. Comparison of the observed signal with the synthetic signal produced by idealized circular eddies suggests that the rotational events can be associated with the passage in the southwestward direction of cyclonic and anticyclonic eddies of diameter similar to the mooring distance. Eddy diameters are, thus, a few tens of kilometers while the propagation speed as obtained from the idealized eddy considerations is estimated to be about 10–15 cm/sec.

[42] Following *Lilly and Rhines* [2002], estimates of characteristic parameters were made. Specifically, from the two outermost moorings mainly involved in the passage of mesoscale eddies, advection speed and direction, peak azimuthal velocity, eddy radius and Rossby number were calculated for each cell, and then vertically averaged. Advection velocity was typically below 15 cm/sec and directed prevalently southwestward, while the eddy peak azimuthal velocity varied between 12 and 21 cm/sec. The Rossby number was predominantly between 10^{-2} and 10^{-1}, meaning that the flow can be considered linear to a first approximation. Cyclonic and anticyclonic eddies had similar radii, i.e., between 10 and 18 km, although cyclones seemed to be slightly larger, travel faster and occupy larger depths than anticyclones. The centers of the eddies generally passed close to the central V3 station.

[43] Eddies are likely formed through the stretching of the high potential vorticity water column, the same mechanism encountered in the Denmark Strait and associated with the dense water overflow [*Spall and Price*, 1998]. In fact, as mentioned, our current meter mooring transect is located about 100 km downstream of the Otranto sill and thus the water column above the AdDW layer is subjected to stretching due to the depth increase and dense water deepening. Starting from this hypothesis and following *Spall and Price* [1998], we determined the spatial and temporal scales of the eddies as a function of the density difference between the intermediate and bottom layers, and of the bottom slope. The density difference between the AdDW and the intermediate layers as obtained from historical experimental in situ data at the Otranto sill had a value of 0.06 kg/m^3. This value, according to theoretical calculations of *Spall and Price* [1998], corresponds to an eddy length scale of about 30 km and a timescale of about 7 days. Applying the second criterion, the same scales were obtained with the value of the local bottom slope of 1.2×10^{-2}, calculated to the north of the measurement section.

[44] The baroclinic instability of the overflow layer as presented in *Kida et al.* [2009] may also possibly be responsible for the eddy formation in the Strait of Otranto. This instability then gives rise to the eddy variability over the entire water column. Obviously our measurements covered only the overflow layer or a part of it, and thus we cannot conclude anything about the vertical extension of eddies over the rest of the water column. Also, due to the incomplete coverage of the water column by the current measurements, we were not able to estimate possible entrainments that can double the overflow as shown in *Voet and Quadfasel* [2010].

[45] Thermohaline properties recorded above the seabed for the three moorings show that the passage of cyclones is associated with higher density (lower temperature and lower salinity), which was explained in terms of upwelling in their centers. Moreover, the density changes can be partly attrib-

uted to entrapment of waters residing upstream of the transect area and their advection by eddies southward. On the other hand, anticyclones were associated with the downwelling in their centers and consequently with the presence of lower density (higher temperature and higher salinity) waters. Finally, it was shown that cyclonic eddy passages and associated strong eastward flow at the front part of the eddies may cause sediment transport seaward from the continental slope area.

[46] **Acknowledgments.** We thank D. Deponte, P. Mansutti, and other members of the technical team of OGS for their contribution during the current measurement and data preprocessing phases. The captains and the crews of the R/V *Universitatis* and R/V *Explora* are acknowledged for their collaboration during the deployment and recovery operations at sea. We are thankful to I. Tomini for providing a high-resolution bathymetric map of the Strait of Otranto. This study was carried out within the Italian national VECTOR project.

References

Bruce, J. G. (1995), Eddies southwest of the Denmark Strait, *Deep Sea Res., Part I*, *42*(1), 13–29, doi:10.1016/0967-0637(94)00040-Y.

Ferentinos, G., and N. Kastanos (1988), Water circulation patterns in the Otranto Straits, eastern Mediterranean, *Cont. Shelf Res.*, *8*(9), 1025–1041, doi:10.1016/0278-4343(88)90037-4.

Flagg, C. N., J. A. Vermersch, and R. C. Beardsley (1976), New England Shelf dynamics experiment (March, 1974) Data Report Part II: The moored array, *Rep. 76-1*, Mass. Inst. of Technol. Cambridge, Mass.

Gačić, M., V. Kovačević, B. Manca, E. Papageorgiou, P.-M. Poulain, P. Scarazzato, and A. Vetrano (1996), Thermohaline properties and circulation in the Strait of Otranto. Dynamics of Mediterranean straits and channels, *Bull. Inst. Oceanogr.*, *17*, 117–145.

Kastanos, N., and G. Ferentinos (1991), Mesoscale current variability in the Otranto straits, Adriatic Sea, *J. Geophys. Res.*, *96*(C5), 8741–8754, doi:10.1029/89JC03262.

Kida, S., J. Yang, and J. F. Price (2009), Marginal sea overflows and the upper ocean interaction, *J. Phys. Oceanogr.*, *39*, 387–403, doi:10.1175/2008JPO3934.1.

Kovačević, V., M. Gačić, and P.-M. Poulain (1999), Eulerian current measurements in the Strait of Otranto and in the southern Adriatic, *J. Mar. Syst.*, *20*, 255–278, doi:10.1016/S0924-7963(98)00086-4.

Lilly, J. M., and P. B. Rhines (2002), Coherent eddies in the Labrador Sea observed from a mooring, *J. Phys. Oceanogr.*, *32*, 585–598, doi:10.1175/1520-0485(2002)032<0585:CEITLS>2.0.CO;2.

Manca, B. B., V. Kovačević, M. Gačić, and D. Viezzoli (2002), Dense water formation in the southern Adriatic Sea and spreading into the Ionian Sea in the period 1997–1999, *J. Mar. Syst.*, *33–34*, 133–154, doi:10.1016/S0924-7963(02)00056-8.

Manca, B. B., G. Budillon, P. Scarazzato, and L. Ursella (2003), Evolution of dynamics in the eastern Mediterranean affecting water mass structures and properties in the Ionian and Adriatic Seas. *J. Geophys. Res.*, *108*(C9), 8102, doi:10.1029/2002JC001664.

Preisendorfer, R. W. (1988), *Principal Component Analysis in Meteorology and Oceanography, Dev. Atmos. Sci. Ser.*, vol. 17, 425 pp., Elsevier, New York.

Spall, M. A., and J. F. Price (1998), Mesoscale variability in the Denmark Strait: The PV outflow hypothesis, *J. Phys. Oceanogr.*, *28*, 1598–1623, doi:10.1175/1520-0485(1998)028<1598:MVIDST>2.0.CO;2.

Ursella, L., V. Kovačević, D. Deponte, and M. Gačić (2007), Analisi dei dati storici di corrente nel canale di Otranto e nel sud dell'Adriatico acquisiti durante il progetto MATER nel periodo 1997–1999, *Rel. OGS 2007/109 OGA 32 OCE*, 70 pp. (Available from OGS, B.go Grotta Gigante 42/c 34010 Sgonico (Ts), Italy; lursella@ogs.trieste.it)

Ursella, L., et al. (2011), Low-frequency flow in the bottom layer of the Otranto Strait, *Cont. Shelf Res.*, in press.

Voet, G., and D. Quadfasel (2010), Entrainment in the Denmark Strait overflow plume by meso-scale eddies, *Ocean Sci.*, *6*, 301–310, doi:10.5194/os-6-301-2010.

Whitehead, J. A., M. E. Stern, G. R. Flierl, and B. A. Klinger (1990), Experimental observations of baroclinic eddies on a sloping bottom, *J. Geophys. Res.*, *95*, 9585–9610.

Williams, R. G., and M. J. Follows (1998), Eddies make ocean deserts bloom, *Nature*, *394*, 228–229, doi:10.1038/28285.

M. Gačić, V. Kovačević, and L. Ursella, Istituto Nazionale di Oceanografia e di Geofisica Sperimentale, Borgo Grotta Gigante 42/C, I-34010 Sgonico, Trieste, Italy. (mgacic@ogs.trieste.it; vkovacevic@ogs.trieste.it; lursella@ogs.trieste.it)